www.lajss.org
Latin American Journal of Solids and Structures 1 (2004) 233–260

Experimental and Numerical Studies of the Collapse of Thin Tubes under Axial Compression

N. K. Gupta and Nagesh

Department of Applied Mechanics
Indian Institute of Technology Delhi, Hauz Khas
New Delhi – 110016, India

Abstract

Experiments on aluminum tubes with varying D/t ratios and their finite element simulation have been performed to study their collapse mechanism as well as the load compression and the energy absorption responses. Convergence studies with respect to model parameters like load step size, mesh density and boundary conditions have been established. Dependence of deformation characteristics and energy absorption response on boundary conditions (end fixity), geometrical parameter- D/t ratio, and material parameters - yield strength and tangent modulus, have been studied. Transition of deformation mode shapes from axisymmetric concertina mode to non axisymmetric diamond pattern owing to tube wall thickness eccentricity under perfectly axisymmetric tube end conditions has been simulated. Validation and comparison of numerical solution with the experimental results have been carried out.

Keywords: Axisymmetric / non-axisymmetric collapse, axial compression, load–compression characteristics, wall thickness eccentricity, aluminum tube

Notation:

t – tube wall thickness
t_0 – maximum tube wall thickness for eccentric tubes
D – tube diameter
L – length of the tube
e – tube wall thickness eccentricity in mm
θ – polar coordinates around tube circumference
u_r, u_θ, u_z – displacement components in cylindrical coordinates
u_x, u_y, u_z – displacement components in Cartesian coordinates

* Corresp. author Email:nkgupta@am.iitd.ernet.in Received 20 March 2004; In revised form 24 March 2004

1 Introduction

Progressive collapse over the tube length, in an axisymmetric concertina mode, a diamond mode or their combination, during axial compression not only gives a large stroke to length ratio but also high specific energy dissipation at a nearly constant mean buckling load and provides an efficient mechanism of absorbing kinetic energy. Thin walled tubes therefore are being used in a variety of ways in energy absorbing systems and their study of large deformation plasto-mechanics is of considerable importance [1] – [5].

Several experimental studies [6], [7], [8] have shown that the mechanism and mode of deformation as well as the load compression curve of a cylindrical tube are highly dependent on the tube D/t ratio, its material constitutive behaviour, geometric imperfections and boundary conditions. Available analyses of the tubes, however, have been mostly for the axisymmetric concertina mode [1], [5], [9]. Assuming the formation of plastic hinges, most of these studies provide upper bound solutions. In these studies the mechanics of deformation, including inside – outside tube folding [9], is assumed and the values of inside, outside or total fold length is determined by minimizing the energy absorbed. Recently numerical tools have emerged that allow a broad range of quasi-static problems to be analysed effectively. Gupta et al. [11] applied the finite element code FORGE2 to simulate the axial compression of the tubes. They used a rigid viscoplastic material behaviour with a 2D model for axisymmetry, and obtained the deformed shapes and crushing load at different stages of the process.

Theoretical or numerical studies of the non-axisymmetric diamond mode of deformation in the available literature are scarce. Marsolek and Reimerdes [12] presented Explicit Finite-Element simulations using LSDYNA 3D with a fine mesh for metallic cylindrical shell structures subjected to axial loading and compared the numerical results with the experimental results. They optimized the geometry of a trigger mechanism to induce a diamond mode of collapse by varying the boundary conditions at the shell circumference.

In this paper experimental and numerical studies on the axial compression of round aluminum tubes of D/t ratio = 29 under quasi-static loading are presented. The deformation process is modeled and simulated for analysis in the finite element code ANSYS using a nonlinear implicit quasi-static analysis. Load deformation and energy absorption characteristics obtained from the numerical models have been compared with the experimental results. Convergence studies with respect to mesh density and proposed reduced sector model and compared with a full 360 degree model have been presented. Dependence of deformation characteristics and energy absorption response on boundary conditions (tube end fixity), geometrical parameter-D/t ratio and material parameters - yield strength and tangent modulus, have also been studied numerically. The effect of eccentricities in wall thickness around the tube circumference on the collapse mode and energy absorption characteristics have been studied numerically under perfectly axisymmetric tube end conditions. These results compare well with the experiments.

2 Experiments

Commercially available round aluminum tubes of diameter = 50.8mm and thickness = 1.74mm (D/t = 29) were obtained and cut to required L/D ratio = 2. Quasi-static axial compression experiments on both as received and annealed tubes were conducted on Zwick / Roelle machine of 25 T capacity and the corresponding load versus cross head movement graphs and energy absorption characteristics are obtained automatically using the interface software on the computer. Fixtures are available, which enable precise load alignment with the geometric center of the tube specimen. Annealing was done by soaking the tubes at 300 deg C in furnace for one hour and cooling these in the furnace for 24 hours. To study the effect of wall thickness eccentricities some of these tubes were incorporated with an eccentricity of about 0.5mm (reduction in thickness) by off center machining. Details of tube dimensions and their modes of deformation are given in Table 1.

Experiments revealed that both annealed and as received tubes deformed in ring mode. Typical load-deformation curves for these specimens are shown in Figure 1(a). The tensile stress strain curves obtained from uniaxial tension tests performed on specimen machined from respective tubes (as per ASTM B 557M) for both as received and annealed state have been shown in Figure 1(b). The specimen were of 50mm gauge length and 12.5mm gauge width, keeping a large transition radius, the grip length was 75mm out of which the actual gripping was about 35mm over a grip width of 20mm. This ensured axial load over the central gauge length. As a result of softening of the material brought about by annealing (reduction in yield strength, Ultimate tensile strength and Elastic modulus) there is a drastic reduction in the load deformation characteristics of the annealed tubes as seen from Figure1(a).

The 50.8mm diameter tubes with L/D = 1.4 and D/t = 29 with induced eccentricity by off center machining collapsed in a diamond mode when subjected to axial loading with an initial axisymmetric fold. Collapse mode of this tube is compared with the pure concertina mode of collapse in its as received state in Figure 2. The collapse of the tube in mixed concertina / diamond mode or diamond mode is seen to result in reduced energy absorption as shown in Figure 3.

3 Numerical Modeling of progressive folding of thin walled tubes

Numerical simulations are carried out using an implicit FE code ANSYS for the quasistatic axial compression of the tubes. The solution scheme incorporated both material and geometric nonlinearities. 20 noded solid elements with 02 elements in thickness direction are used for the discretization of the domain due to superior results and associated contact convergence characteristics in comparison to the 8 noded 3D solid element. To capture the folding process a fine mesh (element edge length < 2.5mm) is used. The material behavior of aluminum is assumed to be elasto-plastic, with a bilinear isotropic material model closely following the experimentally

Material Aluminum	Mean Dia D(mm)	Thickness t (mm)	D/t	L/D	Pm (KN) Mean	Pi (KN) (First Peak)	Pi/Pm	Mode of Deformation	Total Compression (mm)
As Received	50.80	1.74	29.19	2	27.083	43	1.587	Axi symmetric	50
Anealed	50.80	1.74	29.19	2	15.17	23	1.516	Axi symmetric	50
As Received	50.80	1.74	29.19	1.4	27.083	43	1.587	Axi symmetric	40
As Received (eccentric 0.5mm)	50.80	1.74 max 1.24 min	33.33	1.4	19.82	36	1.81	One Fold+ Diamond	40

Table 1: Aluminum tube dimensions with the first peak load "Pi", the mean collapse load "Pm' and collapse mode under axial compression.

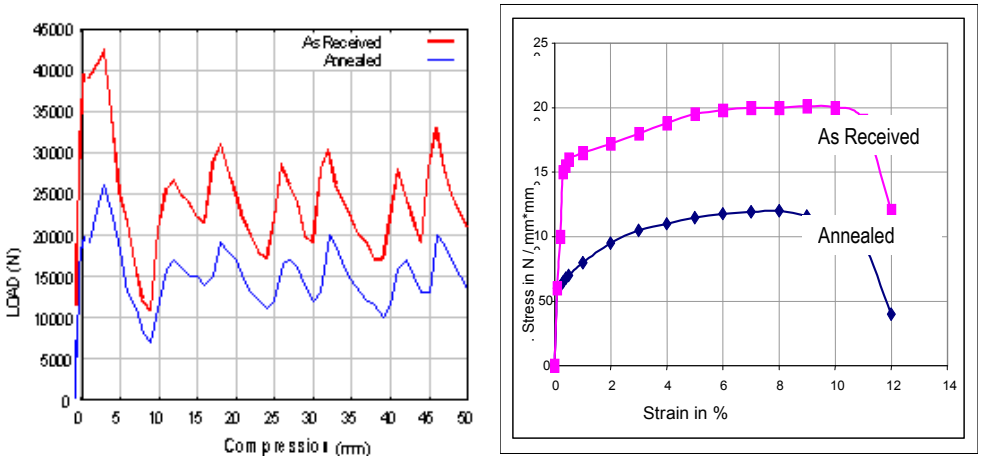

(a) (b)

Figure 1: Experimental curves for as received and annealed specimen (a) Load - Compression curve (b) Stress - strain curves.



(a) As Received (b) Annealed (c) Eccentric

Figure 2: 50.8mm Al tube (a) As received (b) Annealed and (c) With eccentricity in thickness around tube circumference.

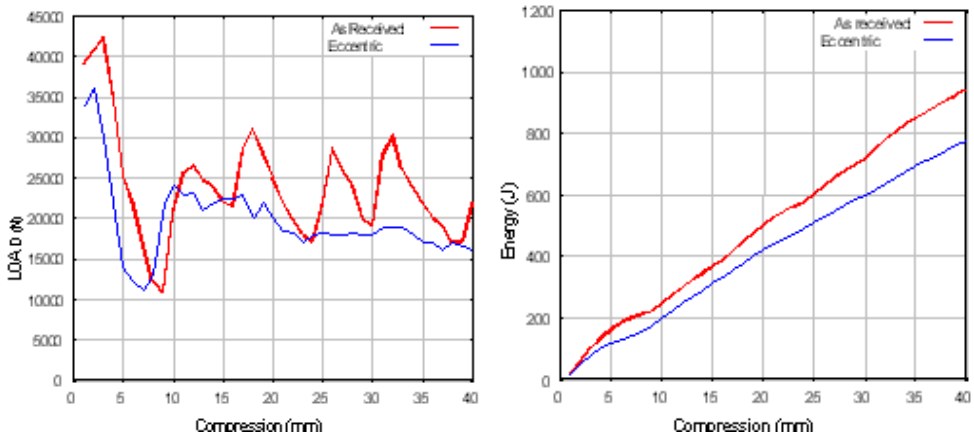

Figure 3: Experimental load deformation and energy absorption curves for as received tubes and 0.5mm eccentric in wall thickness.

established uniaxial stress – strain curve of the material.

The tube models have been parameterised within the ANSYS programming environment and are created in the following sequence. Firstly, a 2D meridian cut of the model in the 0° plane is generated with the desired number of elements in the thickness and the axial direction, initially meshed with 8 noded isotropic shell element. Thereafter the base meshed area is rotated about the origin centre line by the specified sector angle and assigned with the 20 noded 3 D solid brick element for meshing the swept volumes. The cylinder FE models can also be specified as a full 360° model, with symmetry boundary conditions or with coupling conditions in the circumferential direction. The bottom end of the discretised tube model is constrained with axial displacement (z direction), and on its inner periphery the nodes are restrained against circumferential and radial displacement. The axial compression of the tube is simulated by prescribing axial displacement to the nodes at the top end. A non-linear solution scheme is adopted with small incremental axial load steps prescribed.

4 Numerical features of a large deformation simulation

Salient features of the parametric FE model developed in the present study and solution controls in ANSYS are as follows:

1. Non linear solid finite elements that permit large displacements, rotations, curvatures and distortions to be simulated accurately, economically and free from numerical instabilities.
2. Surface to surface contact and target elements for modeling support, self and rigid body contacts.
3. Efficient and flexible solution strategies that permit economic stable and accurate incremental loading with possibility of full or modified Newton Raphson scheme.
4. Results and output reduction and selection
5. Convenient restart features between the load steps (small incremental displacements at one end of tube)
6. Storing data/results for post processing stress plasticity contours, time relationships and deformed shape plots.

5 Boundary conditions and convergence studies

When three-dimensional shell or volume elements are used to model axisymmetric structures under axisymmetric loading it is clearly not appropriate to construct full 360° mesh. The effort for the discretisation in the circumferential direction would be tremendous. If a reduced

sector model is used, the problem of boundary conditions for the sections in the meridian plane arises. In the literature, 90 ° sector models with so-called axisymmetric boundary conditions are frequently encountered. This situation is shown for elements with displacement degrees of freedom in Figure 4 on the left. All arguments presented here hold also for elements with rotational degrees of freedom.

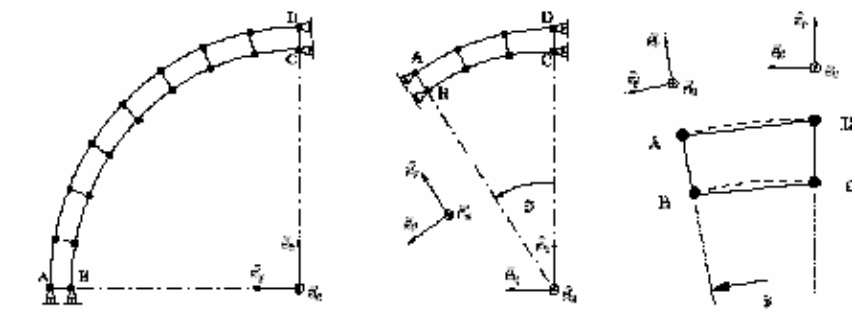

Figure 4: Symmetry Boundary conditions and Coupling Conditions

The boundary conditions shown are actually symmetry boundary condition with respect to two perpendicular planes. They are simple to set up because only displacement components in a global Cartesian coordinate system are involved. In the example shown the following conditions would be enforced at the nodes A, B, C and D respectively: $u_x|_A = u_x|_B = 0$ and $u_y|_C = u_y|_D = 0$. Since these boundary conditions prevent warping of meridian section planes at A–B and C–D artificial stresses are introduced that will not occur in reality. Hence, the predicted stress field will not be axisymmetric. While the observed displacement in circumferential direction is admittedly small, this is not necessarily true for the induced stresses. Users of these types of boundary conditions depend on the fact that the stress perturbation decays at some distance from the boundary.

A sector spanning an arbitrary angle θ is shown in Figure 4 in the middle. Boundary conditions for cyclic symmetry would be defined as follows: $u_\theta|_A = u_\theta|_B = 0$ and $u_y|_C = u_Y|_D = 0$. To set up these conditions, appropriate reference frames must be defined at nodes A and B so that(u_r, u_θ, u_z) are degrees of freedom instead of (u_x, u_y, u_z). These reference frames are, of course, the local bases of the global cylindrical coordinate system. In effect, the relevant stiffness and force components for nodes A and B will be transformed to cylindrical coordinates when the system of equations is created in the finite element process [13]. The question if a 90 ° sector is sufficient to let the induced stresses decay raises the thought why a lower sector angle should not be used in the first place. Coupling conditions in the global cylindrical coordinate system can be used instead to enforce an axisymmetric solution. For this purpose reference frames parallel to the local basis vectors of the cylindrical coordinates are defined at all nodes. Accordingly,

the components of the displacement vector field with respect to these bases, namely (u_r, u_θ, u_z), will be the independent degrees of freedom. All stiffness and force components are transformed to cylindrical coordinates. This is a standard procedure handled by the finite element program system. The following DOF coupling conditions would be used for the example on the right side in Figure 4 :

$$u_r|_A = u_r|_D \quad u_\theta|_A = u_\theta|_D \quad u_z|_A = u_z|_D$$
$$u_r|_B = u_r|_C \quad u_\theta|_B = u_\theta|_C \quad u_z|_B = u_z|_C$$

In effect, the displacement components at nodes A and B are no longer independent degrees of freedom. They are considered to be tied to the corresponding DOFs at the 'master' nodes C and D. This can be achieved within Finite Element procedures by assigning identical equation numbers to sets of coupled DOFs. In this case, stiffness and force components of a coupled DOF will be assembled in the same matrix positions as the components of the associated 'master' DOF.

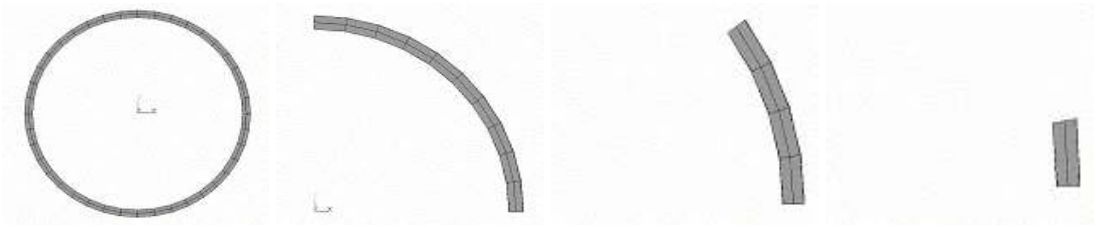

(a) (b) (c) (d)

Figure 5: (a) 360 degree model with 40 elements in circumferential direction, (b) 90 degree model with 10 elements in circumferential direction, (c) 36 degree model with 4 elements along circumference and (d) 9 degree model with 01 element along circumference.

To prove the efficacy of the coupling conditions discussed above FE tube models spanning varying sector angles were made as shown in Figure 5, all with 2 elements in thickness direction. All sector models have their nodal degrees of freedom coupled in the circumferential plane. A nonlinear analysis with nearly 300 load steps over 60mm of axial compression was used for the solution. Multiple pairs of both rigid and flexible contacts have been defined for the FE simulation. The deformation response of the model variants is shown in Figure 6.

The load deflection plots of the tube for the 360° cylinder model and the variants modeled with coupling conditions as shown in Figure 6, there is total agreement between them and are coincident. In case of the model with symmetry boundary conditions, the artificial perturbations are predominant towards the free ends of the cylinder, which result in premature collapse of the numerical model with symmetry boundary conditions.

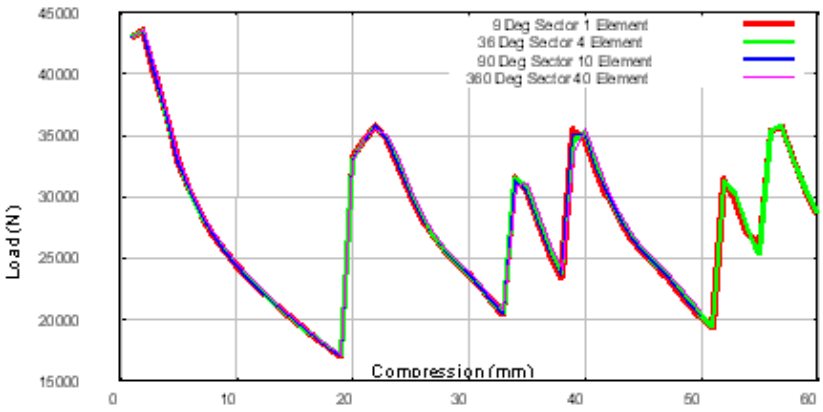

Figure 6: Comparison of the load deformation diagrams till 60mm axial compression in respect of the 04 FE models shown in Fig 5.

Hence, it is inferred that the full 360 ° model of the cylinder can be represented by a small angle, sector model with its nodes coupled in the circumferential direction even for large axisymmetric deformation / progressive concertina mode of collapse. This minimizes the computational effort and resources drastically.

6 Mesh refinement and convergence studies

Convergence studies with increasing mesh density along the length of the tube and in thickness direction with a 20 noded quadratic 3D brick element have been carried out. Convergence is achieved with 2 and 3 elements in thickness direction. Results are at variance with 1 element along thickness and are clearly inadequate to simulate large-scale plastic deformations.

A study was conducted with the help of parameterised cylindrical tubes for comparison of response between 8 noded linear 3D solid elements and 20 noded quadratic 3D solid elements. Convergence is not achieved with linear 8 noded brick elements with increasing elements along the axis in comparison to the 20 noded elements. In case of the quadratic elements the convergence is very good as seen from the load deformation plots in Figure 7 with 40, 50, 60 and 90 elements along the length of the modeled tube.

It is established with convergence studies that the 20 noded quadratic elements are well suited to model the subject large deformation phenomenon and predict a superior correlation with the experimental results in comparison to the 8 noded linear elements. From the computational resource implications it emerges that only one element in circumferential direction is necessary for this kind of analysis, which reduces the computational effort and makes these models affordable

for use on personal computers even for a non-linear analysis. The solution is independent of the number of elements in circumferential direction.

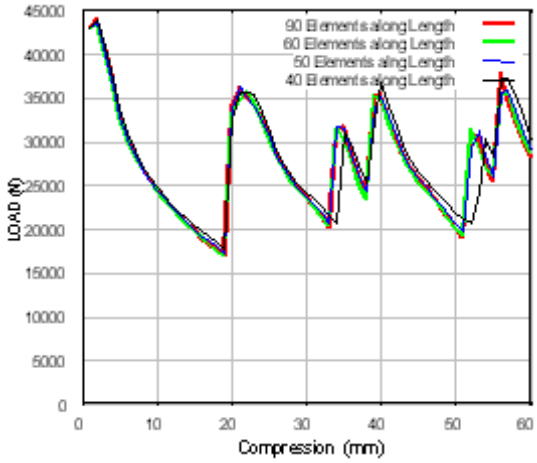

Figure 7: Comparison of the computed load deformation curves 40, 50, 60 and 90 elements in axial direction using 20 noded quadratic 3D brick element.

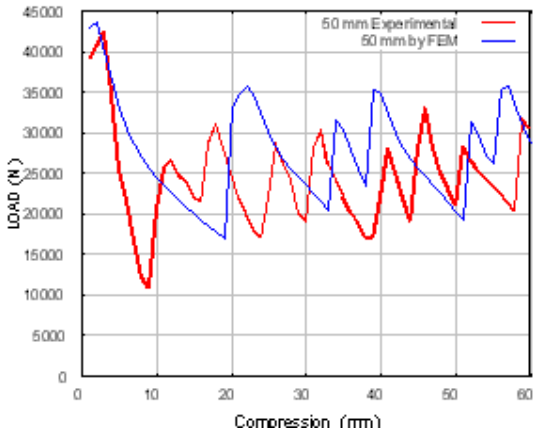

Figure 8: Comparison of experimental and numerical load deformation diagram.

7 Comparison of experimental and numerical results

As observed from comparison of load deformation of FE simulation with experiments as shown in Figure 8, there is good agreement between the first peak and mean load. The pattern of the load deformation curves for the subsequent peaks are also similar. However, the fold formation

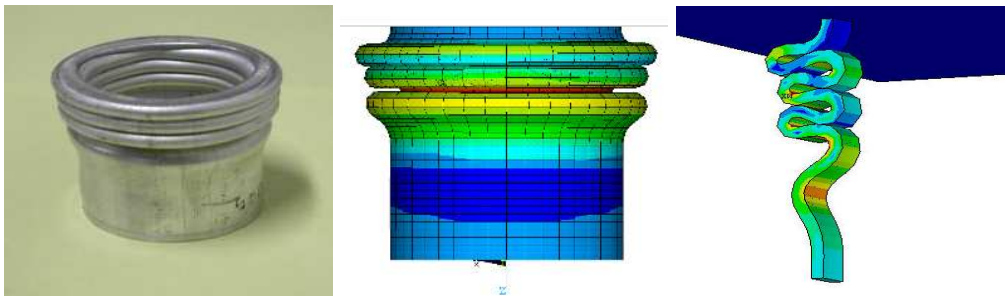

(a) (b) (c)

Figure 9: 50.8mm diameter Aluminum Tubes with (a) 50mm axial deformation, experimental (b) 50mm deformation full 360 degree FEA model (c) 60mm deformation with 9 degree reduced sector FE model.

in FE simulation takes place at a later stage when compared with experiments which may be attributed to the assumptions involved in the discretisation of the continuum in the FE modeling of the structure and variations in the sequence of the contact condition for the FE simulation and experiments. The deformation profiles computed with 360 degrees and 9 degrees sector models are shown in Figure 9 and compared with actual deformed tube.

8 Buckling and folding process of thin walled cylindrical tubes

On reaching a critical buckling load a geometric wave like pattern develops along the length of the tube and the load, which can be carried by the structure, drops. Under the influence of boundary conditions and imperfections an undulation grows into the first plastic fold. The undulations along the length of the cylinder induce the formation of the next fold as shown in Figure 10. The subsequent folds are formed in the same sequence thereby ensuring the progressive folding process to take place. This process results in an oscillating load-compression curve as seen in Figure 11 for both the cases of tube rotation free and restrained, which is characteristic of either an axisymmetric concertina or non axisymmetric diamond shaped folding pattern. The area under this load-compression curve is indicative of the energy absorbed in the progressive folding process which, is affected by the material property, structural geometry, collapse mode, boundary conditions and loading conditions.

Numerical simulations have been useful in studying the deformation mechanism of the axial collapse of tubes by comparing the deformation and stress state at various stages of compression. The deformation characteristics and results have been presented in Figures 11–13 for tube end conditions constrained against rotation and in Figures 14–16 for tubes with end rotations free, at 30 mm compression. The results have been plotted along tube length (S in mm) on the x-axis along the inner (path 1b1) and outer periphery (path 1t2) of the tube wall thickness. The

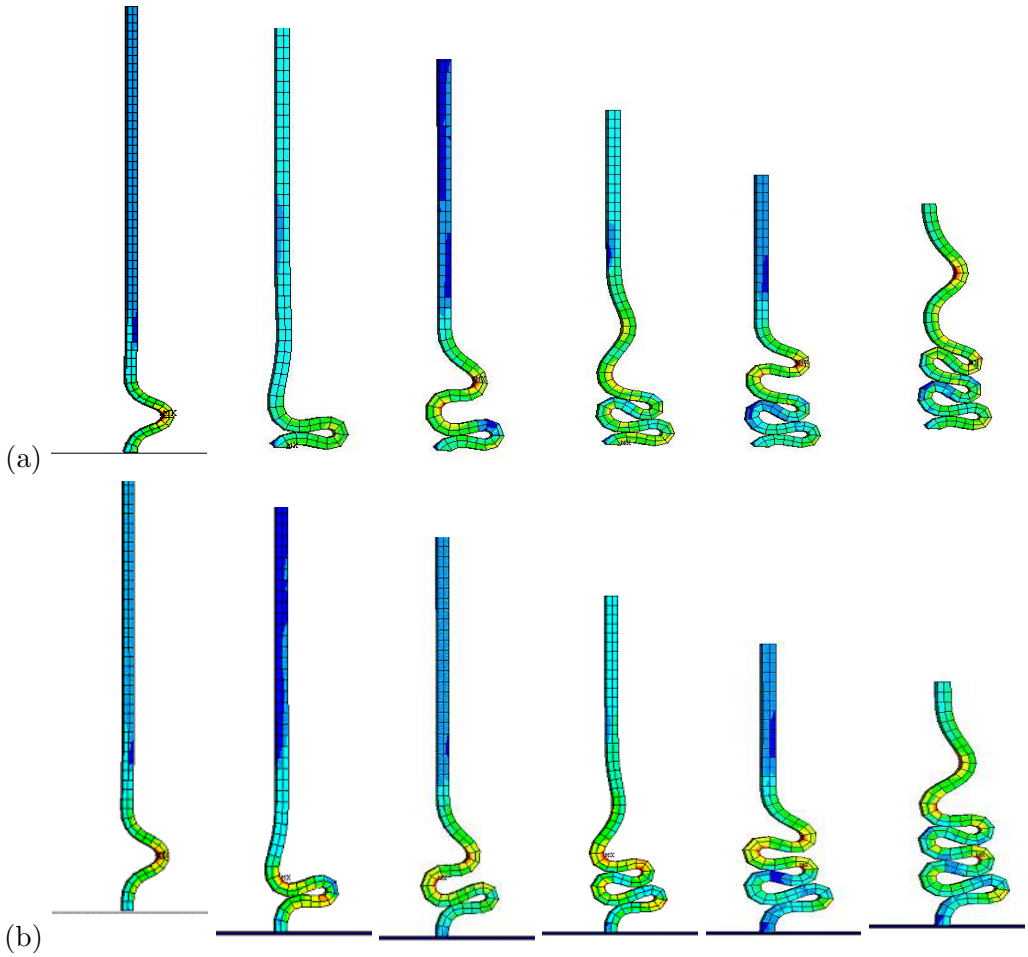

Figure 10: Comparison of computed progressive folding shape of tube for cases (a) end rotation free and (b) end rotation constrained, at 10mm, 20mm, 30mm, 40mm 50mm and 60mm axial compression (from left to right).

deformed tube profile at this stage for both conditions is shown at the third stage in Figure 10.

9 Observations on deformation stages and stress state

From Figures 11 to 16 , it is seen that:

1. The stresses are 3 dimensional in the plastic zone and all the components of normal stresses (axial, circumferential and radial) have large magnitudes in the plastic zone as seen from the result plots for tube end constrained (Figure 11 to Figure 13) and for tube end free to rotate (Figure 14–Figure 16). A membrane state of stress exists away from the plastic zone.

2. Thinning of tube takes place in the regions of plastic hinge as can be seen from Figure 13 and Fig 16 based on the difference in the radial displacement at the inner and outer edge of the tube wall.

3. Cross sectional plane relevant in the folding process is perpendicular to the axial direction and hence the out of plane shear stress σ_{13} has a large magnitude in the plastic zone as observed from Figure 12 and Figure 15.

4. In the region of the plastic zone the bending stresses dominate as evident from the separation between the normal stress at the inside (1b1) and the outside (1t2) of the tube thickness as observed from Figure 11 and Figure 14. Both axial and circumferential bending stresses are present in the plastic zone.

5. The direction of all the components of stress at the inside (1b1) and outside (1t2) of the tube wall changes direction at the plastic hinges between the inside fold and the outside fold.

6. The peaks in the equivalent Von Mises stress is indicative of a plastic hinge which alternates for the inside and outside path corresponding to the inside and the outside fold plastic hinge as seen from Figure 13 and Figure 16.

The fold forms by the development of two plastic zones. The first plastic zone develops fully while second plastic zone develops partially till the formation of first fold is complete. End rotation constraint has a marked effect on the sequence of fold, setting up of contact and plastic hinge formation resulting in the observed changes in the load deformation curve and deformation profile. It is also observed that the ratio of outward fold length to the inner fold length are considerably different for the two cases. For the end rotation constrained this ratio is between 3 and 4 where as for end rotation free the same ratio is between 5 and 6. The numerical results for the outer fold length to inner fold length ratio for the end rotation constrained case compares well with the experimental values reported by Gupta et al. [9].

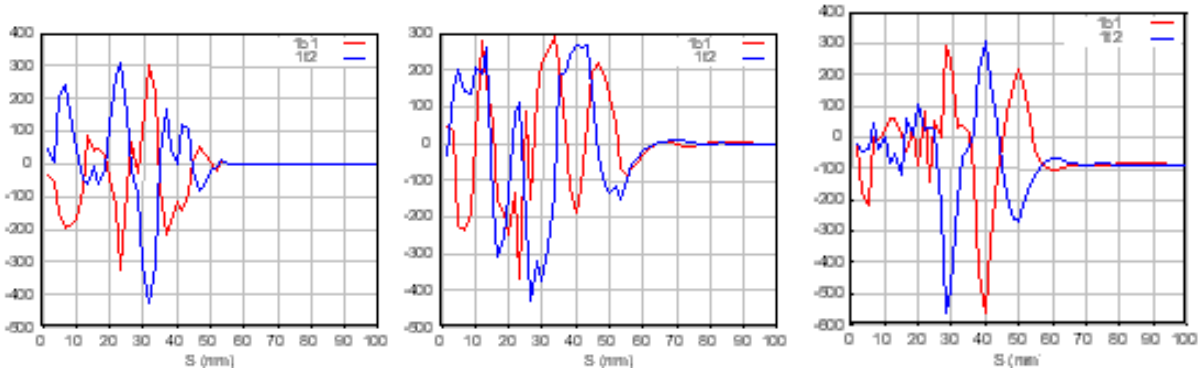

(a) (b) (c)

Figure 11: Normal Stress in (a) axial, (b) circumferential and (c) thickness direction (in MPa) along the length at the inner edge (1b1) and outer edge (1t2) of the tube thickness at 30mm axial compression.

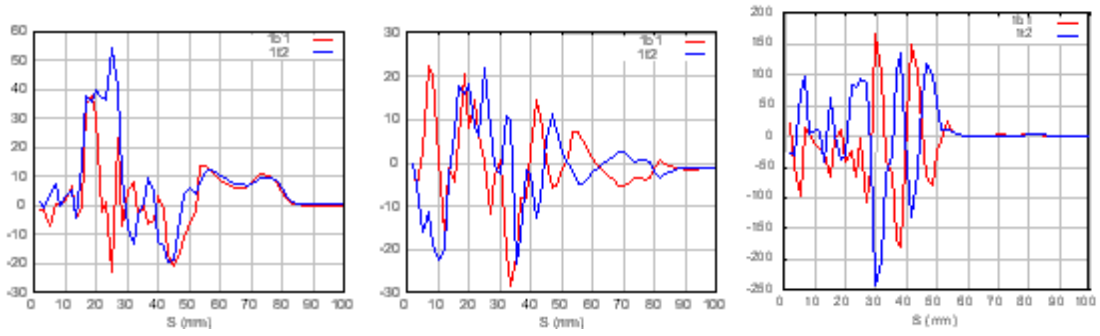

(a) (b) (c)

Figure 12: (a) Inplane shear ($Sigma_{12}$) and (b) Out of plane shear ($Sigma_{13}$) and (c) Out of plane shear ($Sigma_{23}$)) stress in MPa along the length at the inner edge (1b1) and outer edge (1t2) of the tube thickness at 30mm axial compression.

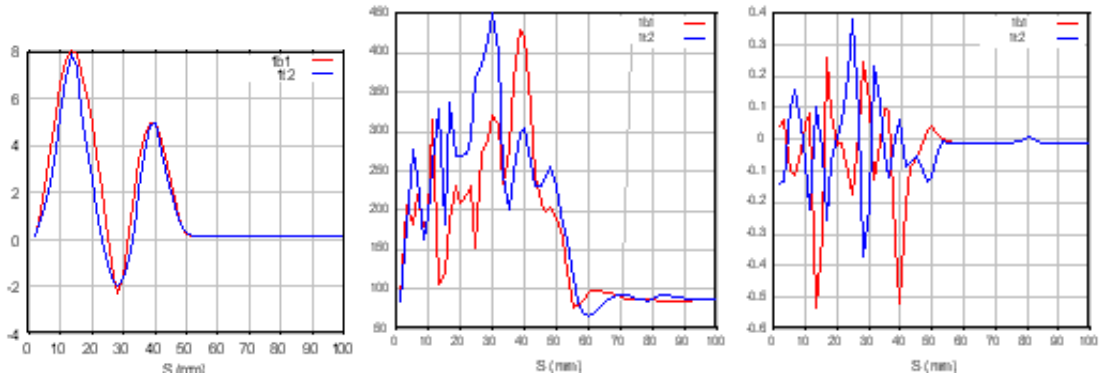

(a) (b) (c)

Figure 13: Radial displacement , (b) Equivalent Von Mises Stress and (c) Normal strain along the length at the inner edge (1b1) and outer edge (1t2) of the tube thickness at 30mm axial compression.

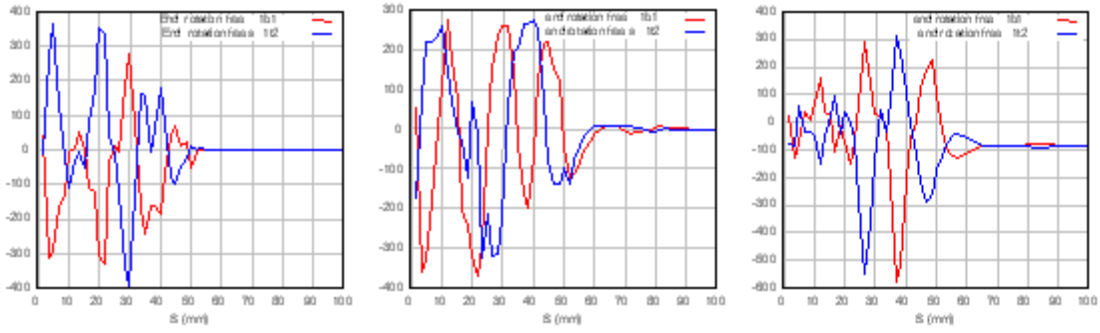

(a) (b) (c)

Figure 14: Normal Stress in (a) axial , (b) circumferential and (c) thickness direction (in MPa) along the length at the inner edge (1b1) and outer edge (1t2) of the tube thickness at 30mm axial compression.

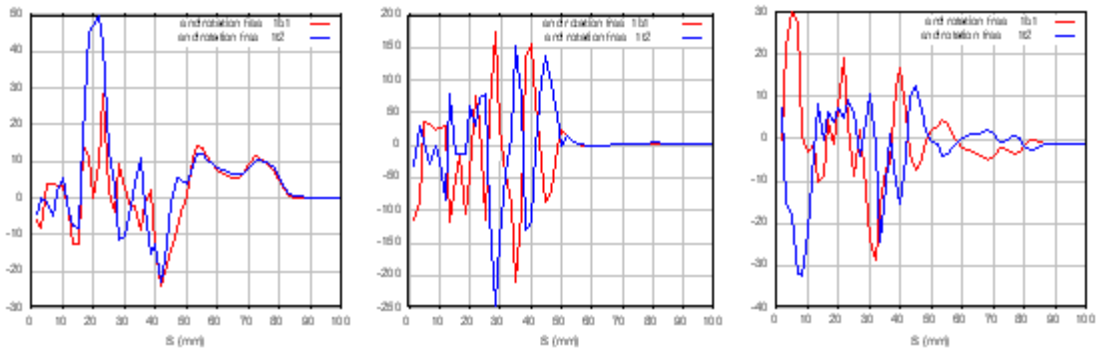

(a) (b) (c)

Figure 15: (a) Inplane shear ($Sigma_{12}$) and (b) Out of plane shear ($Sigma_{13}$) and (c) Out of plane shear ($Sigma_{23}$) stress in MPa along the length at the inner edge (1b1) and outer edge (1t2) of the tube thickness at 30mm axial compression.

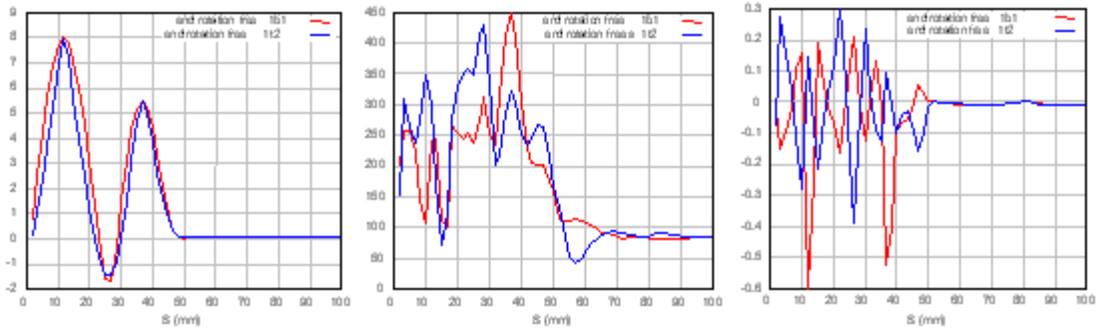

(a) (b) (c)

Figure 16: (a) Radial displacement, (b) Equivalent Von Mises Stress and (c) Normal strain along the length at the inner edge (1b1) and outer edge (1t2) of the tube thickness at 30mm axial compression.

It is observed from the comparison of the load deformation curve of FE simulation with end rotation free and constrained that they are very similar to each other except for the magnitude of successive peak loads which increases for the "end rotation" free model while remaining constant for the "fixed model". The double peaks characteristic of the experimental load deformation curve appears in the "fixed model" but at a later stage of axial compression in comparison to the experiments (Figure 17). The double peaks are missing in the FE model with end rotation free. The FE model with end rotation restrained simulates the experimental load deformation curve more closely in comparison to the FE model with end rotation free. The energy absorption during the folding process as simulated by the FE models has a good agreement with the experimental curve.

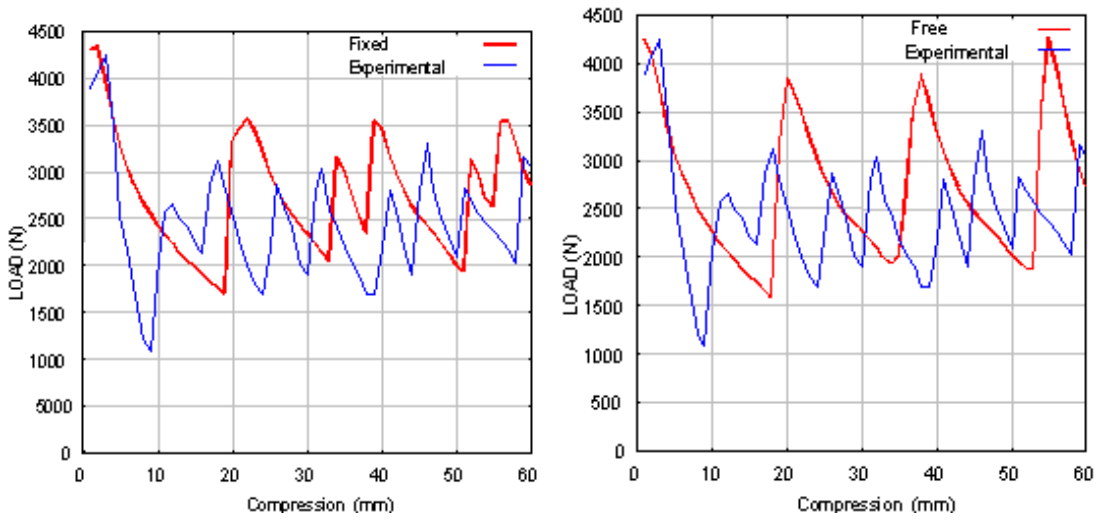

(a) (b)

Figure 17: Comparison of experimental load-compression curve with the curve obtained from FE simulation with (a) tube end restrained against rotation and (b) tube end free to rotate.

10 Variation of deformation and energy absorption response with geometrical parameters

10.1 D/t ratio: constant diameter and varying thickness

The D/t ratio ranging from 20.32 to 50.8 was investigated for load deformation, Energy absorption and folding pattern characteristics using FE simulation and axisymmetric progressive buckling. The diameter was kept constant at 50.8mm and wall thickness varied from 1mm to 2.5mm over the given D/t ratio. The material model was bilinear isotropic with Yield strength of 155 MPa, E = 66450 MPa and Tangent Modulus = 500 MPa for all the cases of D/t. Load

compression characteristics with changing D/t ratio are shown in Figure 18.

As the D/t ratio increases the peak load and mean load decreases. The characteristic double peaks associated with a single tube wall fold becomes single peak as the D/t ratio decreases. The number of fold formed in a given amount of axial compression also decreases with decrease in D/t ratio. Pi and Pm show a nonlinear variation with increasing D/t ratio. Both Pi and Pm decrease with increasing D/t ratio as shown in Figure 10.1.

10.2 D/t ratio: constant thickness and varying diameter

In this study the tube thickness was kept constant at 1.74mm and its diameter varied from 35.34mm to 80mm over the given D/t ratio. The material model was same as in section 10.1 for all the cases of D/t ratio. Load compression characteristics with changing D/t ratio are shown in Figure 20. As the D/t ratio increases the peak load and mean load increases (Figure 21). However, it is observed that there is no correspondence between same load deformation and energy absorption characteristics of tubes same D/t ratio with varying thickness (constant diameter) and tubes with varying diameters (constant thickness).

11 Variation of deformation and energy absorption response with material parameters

11.1 Tangent modulus

The geometry parameters of the investigated FE models were diameter = 50.8mm, thickness = 1.74mm, D/t = 29.29 and L/D = 2. The tangent Modulus was varied from 200 MPa to 1500 MPa to study the variations in load deformation, Energy absorption and folding pattern characteristics using FEA for axisymmetric progressive buckling with change in Tangent modulus. The material model was bilinear isotropic with Yield strength of 155 MPa, E = 66450 MPa for all the cases. The load deformation curve characteristics are very sensitive to the value of the tangent modulus as seen from Figure 22. As the Et increases the peak load and mean load also increases (Figure 23). The extent of folds formed in a given amount of axial compression also decreases with increase in Tangent Modulus.

11.2 Yield strength

In this study the yield strength has been varied from 100 MPa to 225 MPa to study the variations in load deformation, energy absorption and folding pattern characteristics using FEA for axisymmetric progressive buckling with change in Yield point. The material model was same as in section 11.1 for all the cases. It was established that as the yield strength increases for a given tube geometry the peak load and mean load also increases. The load deformation curve characteristics are sensitive to the value of yield strength and both Pi and Pm show a linearly increasing variation with increasing yield point.

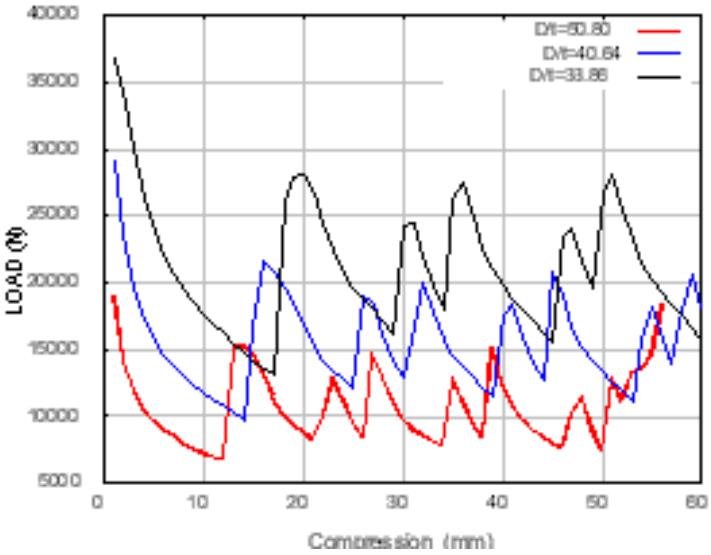

Figure 18: Comparison of Load Deformation diagrams for axisymmetric progressive buckling with varying D/t ratios.

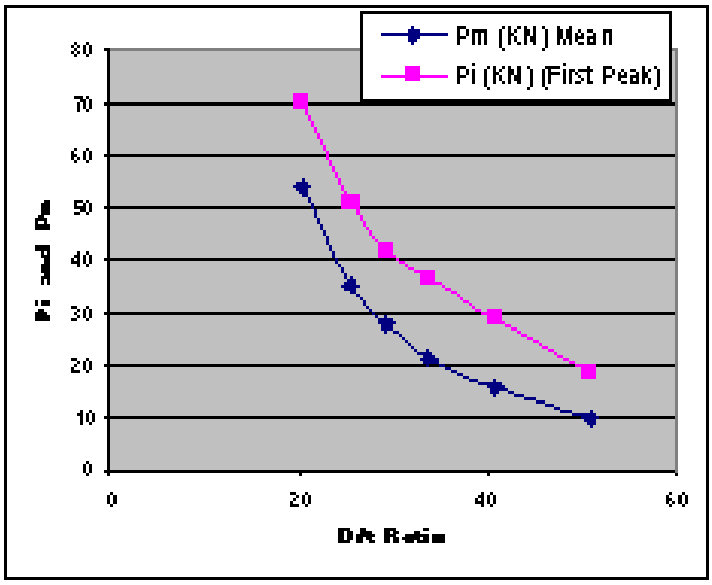

Figure 19: Variation of Pi and Pm with D/t ratio.

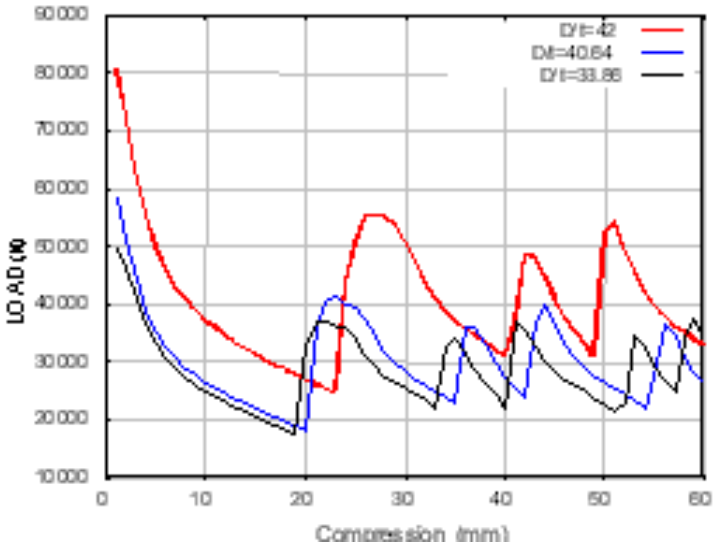

Figure 20: Comparison of Load Deformation diagrams for axisymmetric progressive buckling with varying D/t ratios (constant thickness).

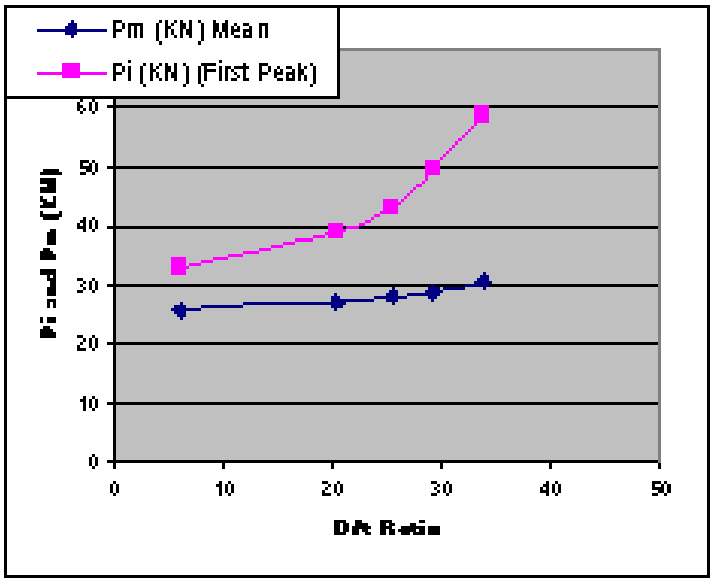

Figure 21: Variation of Pi and Pm with D/t ratio.

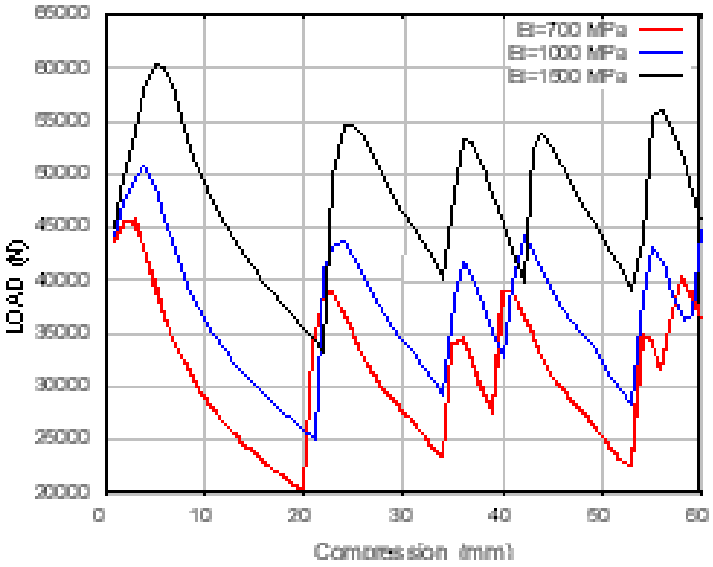

Figure 22: Comparison of Load Deformation diagrams for axisymmetric progressive buckling with varying tangent modulus.

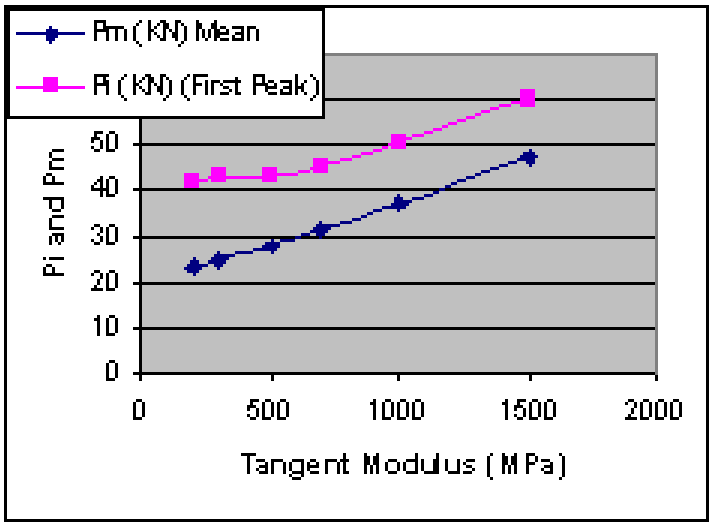

Figure 23: Variation of Pi/Pm with tangent modulus.

12 Large deformation response under axial compression with tube imperfections

The single and most important conclusion of all the theoretical investigations of cylindrical shells is that the primary reason for discrepancy between theoretical critical loads and buckling loads is that the system is extremely sensitive to initial geometric imperfections [14]. The other possible source of discrepancy is the effect of load eccentricities and boundary conditions especially the inplane type [14]. The imperfections and defects that effect the response can broadly be categorized as:

1. Initial geometric imperfections
2. Imperfections in Boundary Conditions (inplane)
3. Material or construction defects.

The geometric shape imperfection may be in the form of a local bubble in a thin cylinder, which makes the geometry locally unsymmetric. It can also be a global out of roundness of varying configurations around the circumference. Imperfections may also be in the wall thickness around the tube circumference, which may be termed as global wall thickness imperfection.

In this paper the influence of wall thickness eccentricity on the mode of deformation was investigated with 50.8mm diameter tube. The wall thickness eccentricity was introduced around the circumference of the as received 50.8mm diameter tube through off center machining. The collapse mode is a mix of concertina and diamond as shown in Figure 24.

The numerical modeling of thickness eccentricity e = 0.5mm has been shown in Figure 25. To match the observed variations in tube wall thickness one half of the tube is modeled with a constant tube thickness. The other half is modeled with a gradual reduction in thickness as governed by:

$$t = t_0 - e \sin\theta \tag{1}$$

t : thickness of the tube wall at a given θ

t_0 : Max Wall thickness as measured

e : tube wall thickness eccentricity = (t max – t min) around the tube circumference

There is no variation in thickness along the length of the tube. The discussed global geometric imperfection is parameterized as a function of the specified 'e' in the finite element model of the tube. The required variation in the thickness around circumference is incorporated into the discretised domain by unchecking the FE mesh from the solid model and updating the nodal coordinates as given by ' t '. The boundary at one end of the tube is restrained against rotation. The axial and circumferential displacements are also arrested.

The thickness eccentricity modeled numerically accounts for the transition to diamond collapse mode, which is at variance with the normally observed collapse mode for this range of D/t ratio. Good correlation is observed between the experimental results and the numerical model

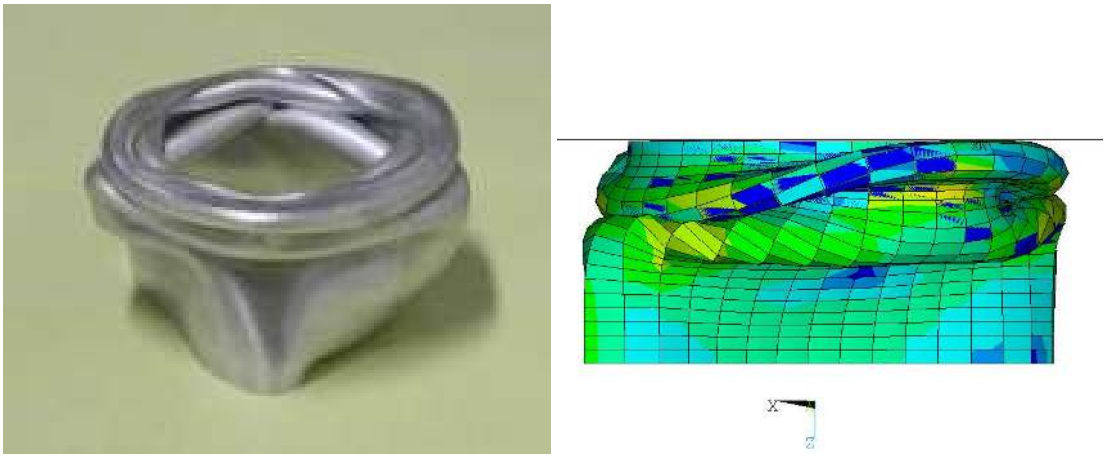

Figure 24: (a)Experimentally deformed 50.8mm diameter tube machined with 0.5mm thickness eccentricity at 40mm axial compression.(b)50.8mm tube numerically modeled with 0.5mm thickness eccentricity at 40mm axial compression.

for the load deformation response of the 50.8mm tube with machined 0.5mm thickness eccentricity around the circumference as shown in Figure 25(b). The collapsed tube in experiments and numerical simulation in a mixed concertina and diamond mode after 40mm axial compression have been compared in Figure 24.

13 Collapse mode sensitivity to e/t ratio (tube wall thickness eccentricity to wall thickness ratio) with axisymmetric tube end conditions

The sensitivity of the collapse mode shape to increasing wall thickness eccentricity in a single lobe for the 50.8mm diameter tube with L/D = 1.4 was studied numerically. The eccentricities of 0.03mm, 0.1mm, 0.2mm, 0.3mm , 0.4mm and 0.5mm for a wall thickness of 1.74mm was studied. The ends of the tube were restrained against rotation and inplane radial and circumferential displacement (axisymmetric end conditions).

As seen from Figure 28 as the level of wall thickness eccentricity increased the tendency to collapse in a diamond mode is also increasesd. It was also observed that the tubes collapsed in a largely axisymmetric concertina mode for wall thickness eccentricity less than 0.1mm for the 50.8mm diameter tubes. The load deformation characteristics with increasing wall thickness eccentricity is shown in Figure 29. The energy absorption capability of the tubes under axial compression showed a decreasing trend with increasing tube wall thickness eccentricity. Both Pi (first peak load) and Pm (average peak load) decrease linearly with increasing eccentricity as shown in Fig 30.

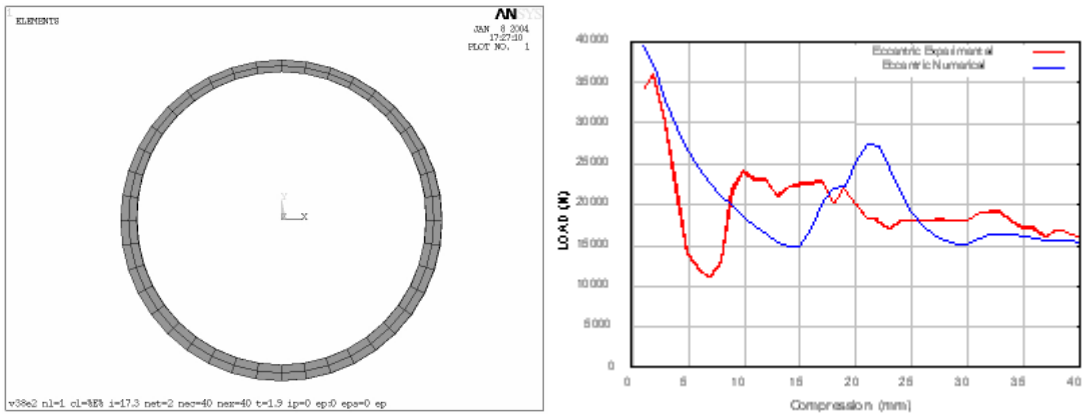

(a) (b)

Figure 25: (a) Tube with 0.5mm Tube wall thickness eccentricity around circumference.(b) Comparison of the experimental and numerical load-compression response of the eccentric tube under 40mm axial compression.

14 Conclusions

Nonlinear FE simulations of quasi-static axial compression of cylindrical tubes deforming in axisymmetric and nonaxisymmetric modes are presented. Convergence studies of the numerical model to parameters like load step size, mesh density, element type and boundary conditions have been investigated in detail. For the axisymmetric collapse it has been established that a thin sector model with only one element and with coupling conditions in circumferential direction, can be effectively used to represent the large deformation response of the entire structure. However, for the non-axisymmetric mode of collapse a full 360 degree FE model of the cylinder is essential. Experimentally observed deformed shapes of the folding process agree well with the numerical simulation results for both axisymmetric and nonaxisymmetric folding of the tubes.

In the present work using the FE analysis regions of plastic hinge, reduced thickness zones, stress state at various stages of deformation and ratio of inside fold to outside fold length are studied in detail. It is observed that the stress state is triaxial in the plastic zone with dominant bending both axial and circumferential. It is observed that load deformation response and hence the energy absorption characteristics are greatly affected by size of the specimen, annealing process and material parameters. The variation in load deformation response is nonlinear with changing D/t ratio. Slope at the onset of yielding (tangent modulus Et) and Yield point affects the load deformation and energy absorption characteristics during a progressive folding process of the tube.

In the studied range of D/t and L/D ratios of the tubes, it is shown through FE simulations that collapse of the tubes in diamond or a mix of concertina and diamond mode is attributed

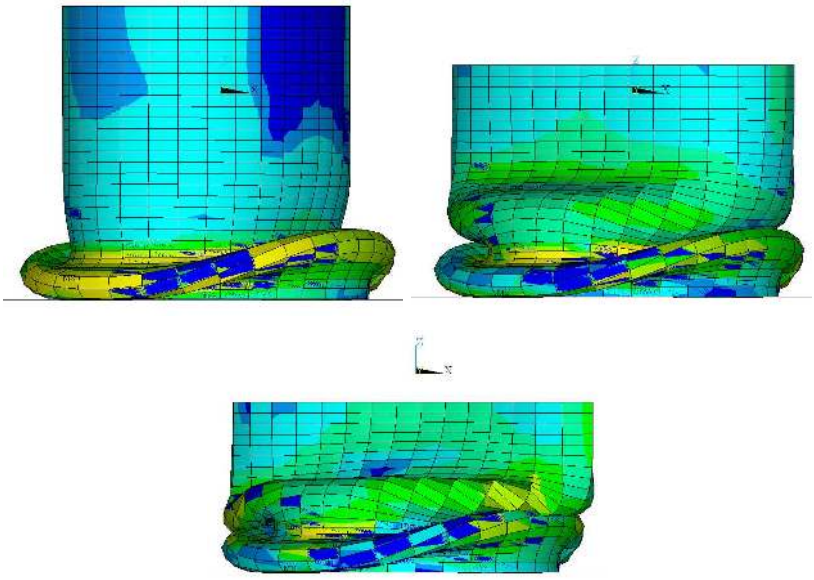

Figure 26: Deformation profiles at 20, 30 and 40mm axial compression of the 50.8mm diameter eccentric tubes using FE simulation

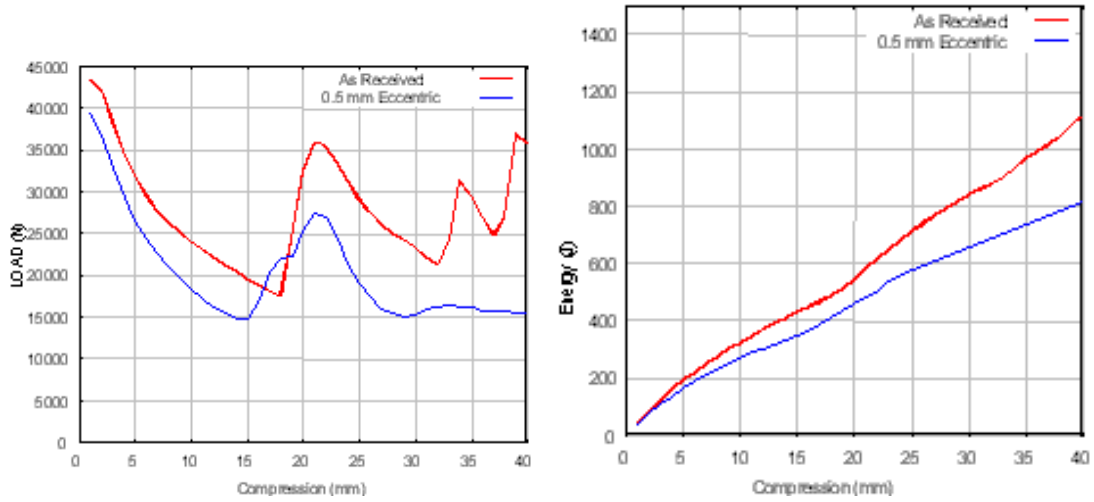

Figure 27: Comparison of the load deformation and energy absorption response using numerical simulation with uniform wall thickness and 0.5 mm thickness eccentricity, under 40mm axial compression.

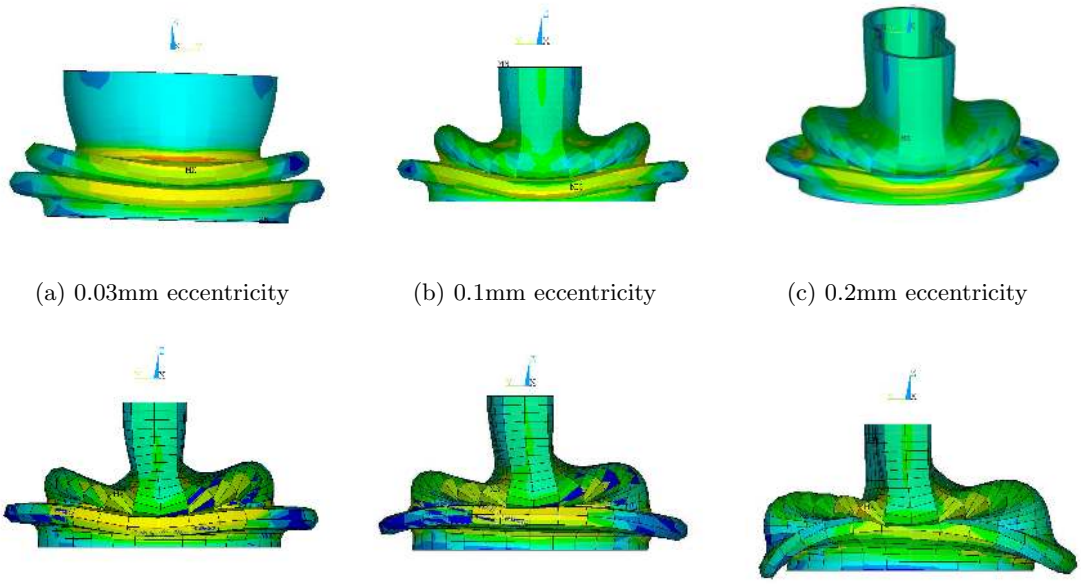

(a) 0.03mm eccentricity (b) 0.1mm eccentricity (c) 0.2mm eccentricity

(d) 0.3mm eccentricity (e) 0.4mm eccentricity (f) 0.5mm eccentricity

Figure 28: Collapse modes and deformation profiles with increasing wall thickness eccentricity at 40mm axial compression.The tube end conditions are perfect axisymmetric.

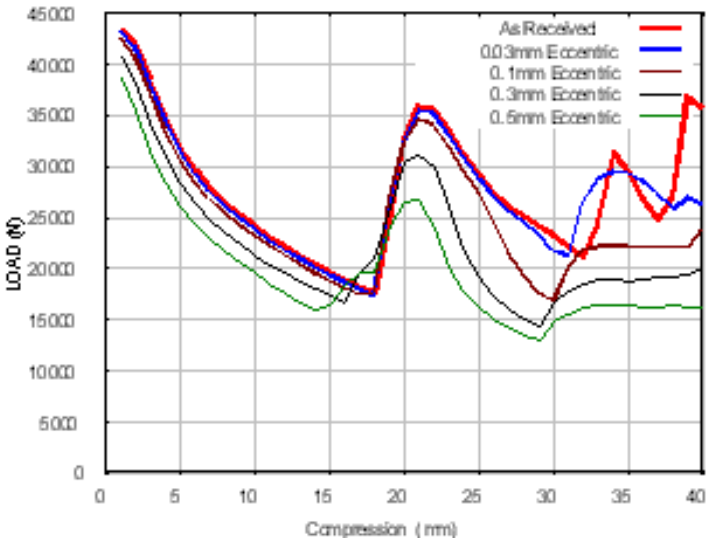

Figure 29: Computed load-compression curves with increasing wall thickness eccentricity

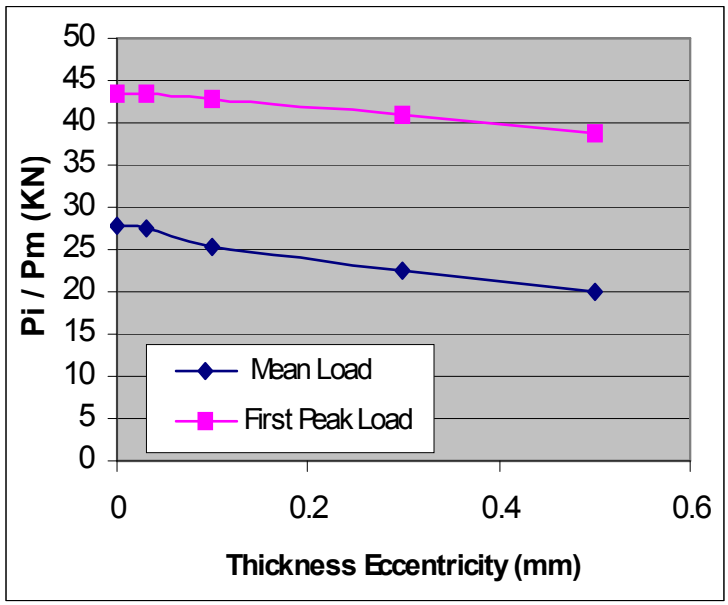

Figure 30: Variation of Pi (First peak load) and Mean Load (Pm) with increasing wall thickness eccentricity.

to imperfections in thickness. Good correlation has been obtained between the experimental results and the numerical model for the load deformation response of the 50.8mm tube with machined 0.5mm thickness eccentricity around the circumference.

The sensitivity of collapse mode to increasing eccentricity has been studied numerically with axisymmetric tube end constraints. It is shown that diamond mode collapse tendency of aluminum tubes under quasi-static axial compression increases with increasing tube wall thickness eccentricity around the circumference. However, the collapse mode is largely concertina for wall thickness eccentricity less than 0.1mm. There is a linear decrease in Pi (First peak load) and Pm (Mean Load) with increasing level of tube wall thickness eccentricity.

References

[1] Alexander, J.M., An approximate analysis of the collapse of thin cylindrical shells under axial loading, Quart. Journal of Mechanics and Applied Maths., 13, 10–15, 1960.

[2] P.H. Thornton, H.F. Mahmood and C.L.Magee, Energy absorption by structural collapse in Structural Crashworthiness, edited by N Jones and T. Wierzbicki, p. 96–114, Butterworths, London, 1983.

[3] S.R. Reid, Plastic deformation mechanisms in axially compressed metal tubes used as im-

pact energy absorbers, edited by N Jones and T. Wierzbicki, p. 1–41, Butterworths, London, 1983.

[4] Wierzbicki, T. and Abramowicz, W, On the Crushing mechanics of Thin Walled Structures, Journal of Applied Mechanics, 50, 727–739, 1983.

[5] Mammalis, A.G. and Johnson, W., The quasi-static crumpling of thin walled circular cylinders and frusta under axial compression, International Journal of Mechanical Sciences, 25, 713–732, 1983.

[6] Andrews, K.R.F., England, G.L. and Ghani, E., Classification of the axial collapse of cylindrical tubes under quasi-static loading, International Journal of Mechanical Sciences, 25, 687–696, 1983.

[7] Jones, N. and Abramowicz, W., Static and dynamic axial crushing of circular and square tubes, Proc. Symposium on Metal forming and Impact Mechanics, Pergamon Press Oxford, p. 225, 1985.

[8] Gupta, N.K. and Gupta, S.K., Effect of annealing, size and cutouts on axial collapse behaviour of circular tubes, International Journal of Mechanical Sciences, 35, 519-613, 1993.

[9] Gupta, N.K. and Velmurugan, R., Consideration of internal folding and non-symmetric fold formation in axi-symmetric axial collapse of round tubes, Internatinal Journal of Solids and Structures, 34 (20), 2611-2630, 1997.

[10] A.A. Singace, Axial crushing analysis of tubes deforming in the multi-lobe mode, International Journal of Mechanical Sciences, 41, 865-890, 1999.

[11] N.K. Gupta, G.S. Sekhon, and P.K. Gupta., A study of formation in axisymmetric axial collapse of round tubes, International Journal of Impact Engineering, 27, 87-117, 2002.

[12] J. Marsolek , H.-G. Reimerdes, Energy absorption of metallic cylindrical shells with induced non-axisymmetric folding patterns, IMPLAST 2003, edited by N.K. Gupta, p. 454–464, New Delhi 2003.

[13] Bathe, K.-J., Finite Element Procedures, Prentice-Hall, 1996, New Jersey.

[14] Sinitses George J, Buckling and post buckling of imperfect cylindrical shells: a review, Applied Mechanics Review, 39, 1517–1524, 1986.